

Construction of Various Time-Varying Hamiltonians on Thin-Film Lithium Niobate Chip

Rui Ye,^{1,*} Guangzhen Li^{1,*†}, Shuai Wan^{1,2,3,*}, Xiaotian Xue^{1,*}, Pi-Yu Wang^{1,2,3,*}, Xin Qiao,⁴ LuoJia Wang,¹ Hao Li,¹ Shijie Liu,¹ Jiayu Wang,¹ Rui Ma,⁵ Fang Bo,⁵ Yuanlin Zheng,^{1,6,‡} Chun-Hua Dong,^{2,3,§} Luqi Yuan^{1,||} and Xianfeng Chen^{1,6,7,¶}

¹State Key Laboratory of Photonics and Communications, School of Physics and Astronomy, Shanghai Jiao Tong University, Shanghai 200240, China

²CAS Key Laboratory of Quantum Information, University of Science and Technology of China, Hefei, Anhui 230026, China


³CAS Center for Excellence in Quantum Information and Quantum Physics, University of Science and Technology of China, Hefei, Anhui 230088, China

⁴College of Physics and Electronics Engineering, Northwest Normal University, Lanzhou 730070, China

⁵MOE Key Laboratory of Weak-Light Nonlinear Photonics, TEDA Applied Physics Institute and School of Physics, Nankai University, Tianjin 300457, China

⁶Shanghai Research Center for Quantum Sciences, Shanghai 201315 China

⁷Collaborative Innovation Center of Light Manipulations and Applications, Shandong Normal University, Jinan 250358, China

 (Received 6 November 2024; revised 18 March 2025; accepted 24 March 2025; published 23 April 2025)

Integrated photonics provides an important platform for simulating physical models with high-performance chip-scale devices, where the lattice size and the time dependence of a model are key ingredients for further enriching the functionality of a photonic chip. Here, we propose and demonstrate the construction of various time-varying Hamiltonian models using a single microresonator on thin-film lithium niobate chip. Such an integrated microresonator holds high-quality factor to 10^6 , and supports the construction of the synthetic frequency lattice with effective lattice sites up to 221 under efficient integrated electro-optic modulation. By further applying different bichromatic modulations composed of two radio-frequency signals oppositely detuned from the resonant frequency in the microresonator, we successfully build various time-varying Hamiltonian models, where the temporal features of the dynamic band structures are captured from experimental measurements, highlighting great flexibility and tunability of this integrated chip. Our work presents a photonic chip for simulating versatile time-varying Hamiltonians, which pushes forward quantum simulations and future photonic applications.

DOI: 10.1103/PhysRevLett.134.163802

Recent developments in photonic chips have exhibited their great capability for achieving versatile physical models with highly compact integration and small footprint size [1–5], and enabling novel functionalities with programmable photonic circuits [6,7] toward quantum computing [8–12], high-efficiency frequency conversion [13,14], and high-bandwidth modulation [15,16]. For these on-chip devices, photonic simulations of physical models with the large scale and the on-demand tunability are usually desired to trigger more opportunities for the integrated photonic applications, where the adjustment can be achieved by different fabrications for specific functionality [17], controlled by patterned pump beams [18], or through

cascading electro-optically and thermo-optically controlled elements [6,19–21]. Although programmable waveguide arrays are able to precisely control independent Hamiltonian terms [22], these present configurations that hold time-independent Hamiltonian features are limited to static physical models. Recent updates on curved waveguides on photonic chips mimic the time-dependent evolution of the model along the waveguide direction [23], but the lattice site number is limited due to the small footprint. On the other hand, periodically driven physical systems characterized by time-varying Hamiltonians (i.e., Floquet system), hold profoundly distinctive features and thus inspire strong study interests [24–27], with exotic photonic phenomena including photon-assisted tunneling [28], Floquet topological insulators [29,30], Floquet *PT*-symmetry [31], and Floquet-Bloch oscillations [32].

The recent surge of interest in synthetic frequency dimensions brings more opportunities to integrated photonics for exploring higher-dimensional physics in simple structures with lower-dimensional geometry [33–40].

*These authors contributed equally to this work.

†Contact author: liguangzhen520@sjtu.edu.cn

‡Contact author: ylzhang@sjtu.edu.cn

§Contact author: chunhua@ustc.edu.cn

||Contact author: yuanluqi@sjtu.edu.cn

¶Contact author: xfchen@sjtu.edu.cn

The constructed physical models in the synthetic frequency dimension depend on flexible external modulation, enabling the realizations of rich exotic phenomena across many photonic areas, including programming photonic simulators [37], quantum walk combs [38], coherently driven dissipative solitons [39], and extraction of the topological invariant [40]. Taking advantage of the high-quality (Q) factor, low loss, and dense integration of chip-scale devices based on the lithium niobate on insulator technology [1–4], a synthetic frequency dimension has also been implemented on photonic chips [41–45], demonstrating interesting physics that includes random walks [41], mirror-induced reflection [42], quantum simulators [43], reconfigurable frequency lattices [44], and arbitrary-range coupling models within on resonant peak [45].

In this Letter, we make an important step forward by constructing various time-varying Hamiltonians in a high- Q microresonator fabricated on a thin-film lithium niobate (TFLN) chip. By applying a bichromatic near-resonant electro-optic (EO) modulation with two modulation frequencies oppositely detuned from the resonant frequency, a periodically driven synthetic lattice model with time-varying coupling strength is constructed in the synthetic frequency dimension. Such synthetic lattice supports a large number of sites up to 221, benefiting from the high electro-optic coefficient, low loss, and high quality of the TFLN chip. Following the band structure measurement method in Refs. [33] and [35], we capture the temporal features of the synthetic lattice by observing the band trajectories, where the time-varying coupling strength is manipulated by tuning the external driving signal. We also showcase the capability of the fabricated tunable device for constructing versatile time-varying Hamiltonians by engineering the modulation patterns. Our study presents a proof-of-principle demonstration on simulating the time-varying Hamiltonians in a single photonic chip, which holds great potential for future simulations of periodically driven non-Hermitian models in the integrated photonics [46–49].

We demonstrate the configurable construction of a synthetic frequency lattice supporting various time-varying Hamiltonian models in a racetrack microresonator coupled with a bus waveguide, as sketched in Fig. 1(a), fabricated on the x-cut TFLN photonic chip [50]. The resonant frequency in the microresonator can be expressed by $\omega_n = \omega_0 + n\Omega_R + \sum_{j \geq 2} D_j n^j / j!$, where ω_0 is a reference frequency, n is the index for the n th mode, $\Omega_R / 2\pi$ is the free spectral range (FSR) of the resonator, D_2 denotes the group velocity dispersion, and $D_j (j > 2)$ is related to higher-order dispersion [57]. When $D_j \ll \Omega_R$, the effect of dispersion can be neglected, and the resonant frequency can be approximated as $\omega_n = \omega_0 + n\Omega_R$. A pair of electrodes are placed on both sides of the microresonator, enabling EO phase modulation with modulation frequency Ω_M in the microwave regime. By applying modulation

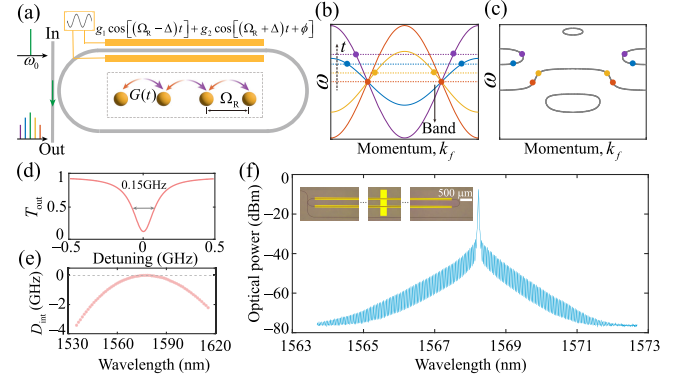


FIG. 1. (a) A racetrack microresonator is driven by a bichromatic near-resonant modulation. The yellow spheres denote the constructed frequency lattice model with time-varying coupling strength $G(t)$ labeled by the color-gradient arrows. (b) Schematic evolution of the static band structures of the system with different times. (c) Schematic band trajectory formed by the intersection points in (b). (d) Through-port transmission spectrum (T_{out}) around the central wavelength 1568.19 nm with full width at half maximum 0.15 GHz. (e) Measured integrated dispersion (D_{int}) as a function of the pump wavelength. (f) The spectrum of the generated EO frequency comb. The inset shows microscope image of the fabricated racetrack microresonator.

$g_0 \cos(\Omega_M t)$ with coupling strength g_0 and $\Omega_M \approx \Omega_R$, a one-dimensional (1D) synthetic lattice along the frequency axis of light is constructed [50]. For $\Omega_M = \Omega_R$, the model gives the energy band as $\varepsilon(k_f) = g_0 \cos(k_f \Omega_R)$, where k_f denotes the wave vector reciprocal to the frequency dimension with units as a time variable [33,35]. However, once we apply a bichromatic near-resonant modulation $J(t) = g_1 \cos(\Omega_{M1} t) + g_2 \cos(\Omega_{M2} t + \phi)$, with $\Omega_{M1} = \Omega_R - \Delta_1$ and $\Omega_{M2} = \Omega_R - \Delta_2$, a time-varying Hamiltonian is constructed [50],

$$H = \sum_n \omega_n a_n^\dagger a_n + J(t) \sum_n \left(a_{n+1}^\dagger a_n + a_n^\dagger a_{n+1} \right), \quad (1)$$

with a_n^\dagger (a_n) being the creation (annihilation) operator for the n th mode. We can set parameters $g_1 = g_2 = g$, $\Delta_1 = -\Delta_2 = \Delta$. After transferring the Hamiltonian into the interaction picture and taking the rotating-wave approximation, we obtain a simplified Hamiltonian,

$$H_C = \sum_n G(t) \left(c_{n+1}^\dagger c_n e^{-i\phi/2} + c_n^\dagger c_{n+1} e^{i\phi/2} \right), \quad (2)$$

with $a_n = c_n e^{-i\omega_n t}$ and $G(t) = g \cos(\Delta t + \phi/2)$. One can see that the Hamiltonian in Eq. (2) describes a tight-binding lattice model with nearest-neighbor (NN) coupling being time-dependent. Such a time-varying Hamiltonian holds a fundamental difference from a static Hamiltonian in quantum mechanisms. To see such difference, we convert the Hamiltonian in Eq. (2) into the k_f space at

each time slice and obtain the instantaneous band structure of the system as

$$\varepsilon_{k_f}(t) = 2G(t) \cos\left(k_f\Omega_R + \frac{\phi}{2}\right). \quad (3)$$

One can see that for a time-varying model, the coupling strength is not constant but varied in time with oscillation period $2\pi/\Delta$. Such time-varying model exhibits the cosinusoidal-shape band feature, while the amplitude of the band oscillates over time holding the same oscillation period with $G(t)$ and oscillation rate being proportional to Δ [see Fig. 1(b)].

To explore such a time-varying Hamiltonian with the periodicity, Floquet theory is usually used [24–27]. For Eq. (2), Floquet analysis results in time-independent and completely flat bands, which are not easy to measure directly [50]. Alternatively, one can track the evolution trajectory of the time-varying band structure using the dynamic band structure method [35]. The main idea is that the system is excited at the linearly varying frequency $\omega(t)$, which hits the dynamic band structure in each time slice, i.e., $\varepsilon_{k_f}(t_m) = \omega(t_m) = 2\pi\eta t_m$, where m is an integer. η denotes the changing rate of the input frequency ω , which represents how fast $\omega(t)$ scans across one resonant dip versus t . At any given time slice t_m , the frequency $\omega(t_m)$ can excite the corresponding eigenvalues on the band $\varepsilon_{k_f}(t_m)$ [the intersection points are labeled by the colored circles in Fig. 1(b)], which are two wave vectors $k_{f,m,1}$ and $k_{f,m,2}$ satisfying Eq. (3). By connecting $[k_{f,m,1(2)}, \varepsilon_{k_f}(t_m)]$ for all time slices, one obtains the trajectory of the dynamic band structure as illustrated in Fig. 1(c).

In experiments, we fabricate the racetrack microresonator on TFLN chip with a circumference of 26.5 mm [see Fig. 1(f)]. We obtain a loaded Q factor of $Q_L = 1.23 \times 10^6$ and measured FSR of $\Omega_R/2\pi = 4.955$ GHz [see Figs. 1(d), S9(b), and S9(c)]. Broadband EO frequency comb generation can be achieved by dispersion engineering [58,59]. The microresonator we design holds very small dispersion around the whole communication band [see Fig. 1(e)], where the measured second-order group velocity dispersion parameter is $|D_2| = 2\pi \times 6$ kHz $\ll \Omega_R$ [50]. The microresonator is then resonantly pumped at wavelength of 1568.19 nm ($\omega_0 = 2\pi \times 191$ THz) with 14 dBm input optical power [see Fig. S9(c)] [50], while the electrodes are under resonant EO modulation $V_0 \cos(\Omega_R t)$ driven by a 20 dBm radio-frequency (rf) signal. An optical frequency comb is obtained with a frequency spanning of 1095 GHz, up to 221 resonant modes, before the comb signal is overwhelmed by local white noise as plotted in Fig. 1(f).

To implement the Hamiltonian in Eq. (2), one can apply a bichromatic EO modulation signal on the electrodes in the form of $V(t) = V_0 \cos[(\Omega_R - \Delta_{\text{exp}})t] + V_0 \cos[(\Omega_R + \Delta_{\text{exp}})t + \phi]$, which is composed by two

radio-frequency signals with their modulation frequencies oppositely detuned from the resonant frequency Ω_R , i.e., $\Delta_1 = -\Delta_2 = \Delta_{\text{exp}}$. To unveil the dynamics in the built synthetic lattice, we perform the dynamic band structure measurement by using the time resolved transmission spectroscopy [see Supplemental Material (SM) [50] Note 5] [33,35]. We linearly scan the pump laser across several FSRs around the central wavelength 1568.19 nm with the frequency scanning rate $v = 2.8$ GHz/ms [50]. A 0.5 ms acquisition of the through-port transmission spectrum (T_{out}) modulated periodically following the modulation frequencies of $V(t)$ is recorded on the oscilloscope, corresponding to a scanning range $0.28\Omega_R \approx 1.4$ GHz. The Brillouin zone of the reciprocal space for the frequency dimension is presented by one round-trip time of the microresonator $T_R = 2\pi/\Omega_R \approx 0.2$ ns [33], where the time within each slice is k_f . We first convert the through-port transmission spectrum T_{out} to the transmission signal S_{out} by $S_{\text{out}} = 1 - T_{\text{out}}$, which is then broken into time slices with fixed time windows. Within each time slice the input frequency can be approximated as unchanged (labeled as ω) and regarded as a fixed input frequency detuning, where one or more transmission peaks are expected in correspondence to those intersection points at which Eq. (3) is satisfied (see Fig. S11 [50]). Therefore, each time slice gives the detection of a band at the energy ω and the wave vector k_f at an instantaneous band. By stacking these time slices vertically as a function of the input frequency, one obtains the trajectory of the time dependently moving band structure.

In the first set of experimental demonstration, we vary $\Delta_{\text{exp}}/2\pi$ from 0, 3, 5 to 10 kHz, where the measured trajectories of the corresponding band structure are shown in Figs. 2(a1)–2(a4). Note that we slice the transmission signal by two round-trip times of the microresonator for better viewing the trajectory over the Brillouin zone in the k_f space, which gives the horizontal periodicity of the band structure $k_f\Omega_R \in [-\pi, 3\pi]$. The system exhibits a static lattice model with $\Delta_{\text{exp}} = 0$ (corresponding to the resonant modulation case where $\Omega_{M1} = \Omega_{M2} = \Omega_R$) for the coupling strength $G(t)$ being a constant, where the band structure exhibits a cosinusoidal shape [see Fig. 2(a1)]. The dynamic feature manifests once the time-varying $G(t)$ in Eq. (3) is built ($\Delta_{\text{exp}} \neq 0$), where the measurements give splitting patterns as shown in Figs. 2(a2)–2(a4). The trajectory of the dynamic band structure associated to different time-varying Hamiltonians is along the vertical energy axis. It also reflects the stationary wave feature of the band structure due to the time-varying coupling strength. The splitting band number increases with the frequency detuning while the vertical energy window remains unchanged. Such splitting results from the eigenvalue of energy at fixed k_f position oscillating faster due to the larger oscillation rate of $G(t)$ when increasing Δ . It leads to more intersection points between the eigenvalue of

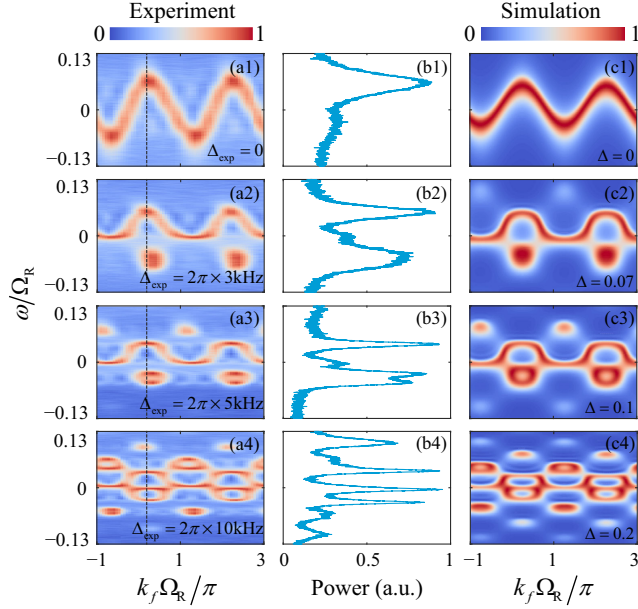


FIG. 2. (a1)–(a4) Measured trajectories of dynamic band structures under EO phase modulation $V(t)$ with varied Δ_{exp} and $\phi = 1.5\pi$. (b1)–(b4) Vertically normalized power distributions at the position $k_f \Omega_R = 0.2\pi$, labeled by the dashed lines in (a1)–(a4). (c1)–(c4) Simulated band trajectories, with different Δ , and $g = 0.4$, $\phi = 1.5\pi$, $\eta = 0.002$.

energy on the band at $k_f \Omega_R = 0.2\pi$ and the input frequency $\omega(t)$ (see Fig. S3 [50]), as seen in corresponding power distributions for the field in Figs. 2(b1)–2(b4), where the peaks label the frequency positions of these intersection points. The oscillation of the eigenvalues can also cause the group velocity of mode spreading along the frequency dimension, leading to Bloch oscillation with oscillation period being $2\pi/\Delta$ (see Fig. S4 [50]). We also simulate the dynamic band structures by solving the coupled-mode equations from the Hamiltonian in Eq. (2) numerically [see Figs. 2(c1)–2(c4)] [50], where the effects from total loss and coupling loss are considered. Note that the simulation parameters Δ , g are normalized in the unit of $\Omega_R/2\pi$, and η is normalized in the unit of $(\Omega_R/2\pi)^2$. It gives the resulting trajectories relatively agreeing well with the experimental results, where the difference between them might result from the disturbance of the environment and experimental devices as well as the approximations used in simulations.

In the Hamiltonian of a one-dimensional lattice model under a constant force [35,41], the phase information does not affect the pattern of band trajectory. It only leads to the shift of band trajectory along the horizontal k_f direction (see Fig. S6), while the resulting Bloch oscillation also remains unchanged when varying ϕ (see Fig. S7) [50]. Nevertheless, the phase in our constructed time-varying Hamiltonian here significantly affects the pattern of band trajectory as shown in Fig. 3, due to the simultaneous influence of phase on the

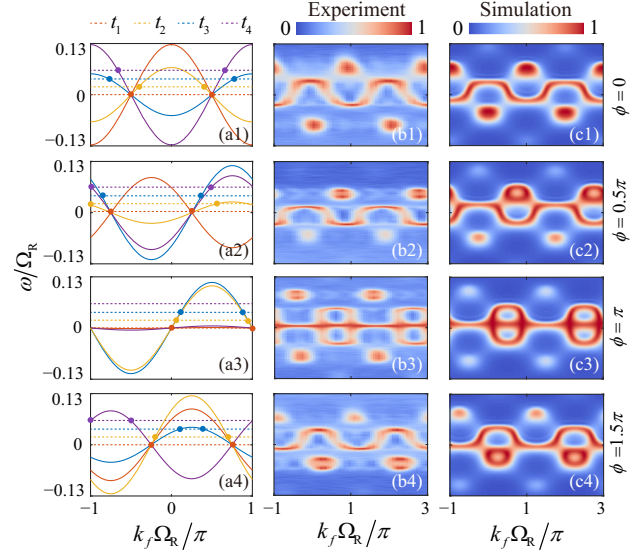


FIG. 3. (a1)–(a4) The evolution of the static band structures of the system in different phase differences ϕ with time varying from t_1 to t_4 . The colored circles label the intersection points of the excitation frequency (dashed lines) and the corresponding static band structure at different times. (b1)–(b4) Measured band trajectories under the same modulation form in Figs. 2(a1)–2(a4) but with varied phase difference ϕ and $\Delta_{\text{exp}} = 2\pi \times 5$ kHz. (c1)–(c4) Simulated band trajectories with different phase difference ϕ , and $g = 0.4$, $\Delta = 0.1$, $\eta = 0.002$. Note in (a3), the purple dashed line at t_4 does not intersect with the purple energy band, so there is no purple circle.

coupling strength $G(t)$ and the static band part $\cos(k_f \Omega_R + \phi/2)$ in Eq. (3). We explain this simple physical picture using the theoretical static band structures at different time slices (t_1, t_2, t_3, t_4) with the fixed $\Delta = 0.1$ and the varying phase difference ϕ in Figs. 3(a1)–3(a4). We see that the bands evolve along the horizontal k_f direction when varying ϕ with a periodicity of 2π , and the shape of $G(t)$ is also modified by ϕ at different time slices. In experiments, we fix $\Delta_{\text{exp}} = 2\pi \times 5$ kHz and change ϕ from 0, 0.5π , π , to 1.5π . The measured band trajectories are plotted in Figs. 3(b1)–3(b4), which matches well with numerical simulations in Figs. 3(c1)–3(c4). The phase information also affects the mode evolution (see Fig. S5), where the mode distribution patterns vary with phases [50]. The measured bands in Figs. 2 and 3 indicate that our experimental setup exhibits relatively low loss benefiting from the high- Q factor of the microresonator, which provides the capability for the on-demand photonic simulations of time-varying Hamiltonians.

Our chip can provide further opportunity for studying more complicated time-varying Hamiltonians. To show such cases, we rewrite the band structure in Eq. (3) to a general form,

$$\varepsilon_{k_f}(t) = g_1 \cos(k_f \Omega_R - \Delta_1 t) + g_2 \cos(k_f \Omega_R + \Delta_2 t + \phi), \quad (4)$$

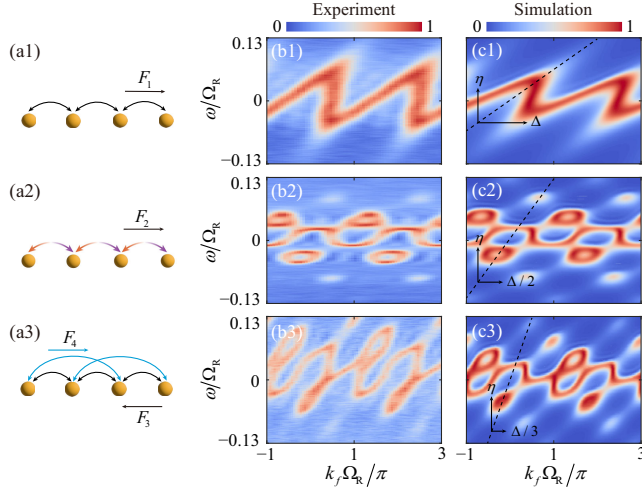


FIG. 4. Synthetic frequency lattice models and measured band trajectories under different combinations of rf signals: (a1), (b1), $V_1(t)$; (a2), (b2), $V_2(t)$; and (a3), (b3), $V_3(t)$, with $\Delta_{\text{exp}} = 2\pi \times 5$ kHz. The arrows in (a1)–(a3) denote the directions of the generated effective external forces. (c1)–(c3) The corresponding simulated band trajectories.

which represents the superposition of two traveling-wave-feature band components. By separately manipulating either one of the two components in Eq. (4), one can obtain arbitrary designed band shapes, corresponding to versatile time-varying Hamiltonians. In experiments, we first consider the single near-resonant modulation with the rf signal having the form $V_1(t) = V_0 \cos[(\Omega_R - \Delta_{\text{exp}})t]$, i.e., the second component in Eq. (4) is zero. It leads to the band structure $\omega_1(t) = V_0 \cos(k_f \Omega_R - \Delta_{\text{exp}} t)$, which corresponds to the model of a 1D photonic lattice under an external force F_1 [see Fig. 4(a1)] [35]. One sees that the band trajectory shifts over time along the k_f axis, as illustrated in the experimental measurement in Fig. 4(b1) and the numerical simulation in Fig. 4(c1). Furthermore, we choose rf signal $V_2(t) = V_0 \cos[(\Omega_R + \Delta_{\text{exp}})t] + V_0 \cos[(\Omega_R - 2\Delta_{\text{exp}})t]$, composed of two near-resonant modulations with asymmetric and unbalanced frequency detunings. It gives the band structure $\omega_2(t) = 2V_0 \cos(3\Delta_{\text{exp}} t/2) \cos(k_f \Omega_R - \Delta_{\text{exp}} t/2)$, which constructs a time-varying lattice under the effective external force F_2 [see Fig. 4(a2)]. It leads to the band structure oscillating along the vertical energy axis while shifting along the k_f direction [see Figs. 4(b2) and 4(c2)]. Lastly, we set $V_3(t) = V_0 \cos[(\Omega_R + \Delta_{\text{exp}})t] + V_0 \cos[(2\Omega_R - 2\Delta_{\text{exp}})t]$, combining both the NN coupling and next-nearest-neighbor coupling near twice the number of FSRs, which gives $\omega_3(t) = V_0 \cos(k_f \Omega_R + \Delta_{\text{exp}} t) + V_0 \cos(2k_f \Omega_R - 2\Delta_{\text{exp}} t)$. This choice of the modulation gives a 1D lattice under two effective external forces F_3 and F_4 with opposite directions along NN and next-nearest-neighbor couplings, respectively [see Fig. 4(a3)], where the

measured and simulated band trajectories are plotted in Figs. 4(b3) and 4(c3). To illustrate the slant of the band structures, we label the slopes of the band patterns by the black dashed lines in Figs. 4(c1)–4(c3), where the horizontal and vertical time dependencies of the band structures are determined by the frequency detunings (Δ) and the changing rate of input frequency (η), respectively. For the cases in Figs. 4(c1) and 4(c2), where only one effective force exists, the slopes are η/Δ and $\eta/(\Delta/2)$, respectively. As for Fig. 4(c3), where two effective external forces exist, the slope is estimated as $\eta/(\Delta/3)$. Similarly, the experimental slant of the band structures is proportional to multiple of v/Δ_{exp} .

In conclusion, we demonstrate the photonic analog of various time-varying Hamiltonian models in a single micro-resonator fabricated on a TFLN chip. By applying the bichromatic EO modulation with two near-resonant modulation frequencies oppositely detuned from the resonant frequency, a high-quality synthetic frequency lattice with time-varying coupling strength is constructed. Such lattice holds a dynamic band structure, where a corresponding evolution trajectory can be tracked in the experiment. We have demonstrated versatile periodically modulated lattice models constructed in the same chip, where band trajectories are measured and verified by simulations. Our work can be potentially extended to explore two-dimensional time-varying Hamiltonian models by coupling multiple high- Q microresonators as additional spatial dimension. In this design, each ring can be manipulated individually, and brings more flexibility and controllable degrees of freedom to the system, where non-Hermitian physics might also be explored if amplitude modulation is integrated [46,49]. By further combining external modulation at the frequency of multiple FSRs to fold the frequency axis of light, the dimensionality of synthetic space might be further increased [37,60,61]. Therefore, our work plays a cornerstone role in exploring higher-dimensional time-dependent physics in photonic chips.

Acknowledgments—The research is supported by National Key Research and Development Program of China (2023YFA1407200 and 2022YFA1205100), and National Natural Science Foundation of China (12104297, 12122407, 12192252, 62022058, 12293052, and 11934012). Y.Z. also thanks the sponsorship from Yangyang Development Fund. This work was partially carried out at the USTC Center for Micro and Nanoscale Research and Fabrication.

Data availability—The data that support the findings of this Letter are openly available [62].

- [1] D. Zhu, L. Shao, M. Yu, R. Cheng, B. Desiatov, C. Xin, Y. Hu, J. Holzgrafe, S. Ghosh, A. Shams-Ansari *et al.*,

- Integrated photonics on thin-film lithium niobate, *Adv. Opt. Photonics* **13**, 242 (2021).
- [2] S. Saravi, T. Pertsch, and F. Setzpfandt, Lithium niobate on insulator: An emerging platform for integrated quantum photonics, *Adv. Opt. Mater.* **9**, 2100789 (2021).
 - [3] Z.-W. Yan, Q. Wang, M. Xiao, Y.-L. Zhao, S.-N. Zhu, and H. Liu, Probing rotated Weyl physics on nonlinear lithium niobate-on-insulator chips, *Phys. Rev. Lett.* **127**, 013901 (2021).
 - [4] Z. Xie, F. Bo, J. Lin, H. Hu, X. Cai, X.-H. Tian, Z. Fang, J. Chen, M. Wang, F. Chen *et al.*, Recent development in integrated lithium niobate photonics, *Adv. Phys. X* **9**, 2322739 (2024).
 - [5] A. Dutt, A. Mohanty, A. L. Gaeta, and M. Lipson, Nonlinear and quantum photonics using integrated optical materials, *Nat. Rev. Mater.* **9**, 321 (2024).
 - [6] W. Bogaerts, D. Pérez, J. Capmany, D. A. Miller, J. Poon, D. Englund, F. Morichetti, and A. Melloni, Programmable photonic circuits, *Nature (London)* **586**, 207 (2020).
 - [7] X. Xu, G. Ren, T. Feleppa, X. Liu, A. Boes, A. Mitchell, and A. J. Lowery, Self-calibrating programmable photonic integrated circuits, *Nat. Photonics* **16**, 595 (2022).
 - [8] J. M. Arrazola, V. Bergholm, K. Brádler, T. R. Bromley, M. J. Collins, I. Dhand, A. Fumagalli, T. Gerrits, A. Goussev, L. G. Helt *et al.*, Quantum circuits with many photons on a programmable nanophotonic chip, *Nature (London)* **591**, 54 (2021).
 - [9] U. A. Javid, J. Ling, J. Staffa, M. Li, Y. He, and Q. Lin, Ultrabroadband entangled photons on a nanophotonic chip, *Phys. Rev. Lett.* **127**, 183601 (2021).
 - [10] H. Mahmudlu, R. Johanning, A. Van Rees, A. Khodadad Kashi, J. P. Epping, R. Haldar, K.-J. Boller, and M. Kues, Fully on-chip photonic turnkey quantum source for entangled qubit/qudit state generation, *Nat. Photonics* **17**, 518 (2023).
 - [11] H. Zeng *et al.*, Quantum light generation based on gan microring toward fully on-chip source, *Phys. Rev. Lett.* **132**, 133603 (2024).
 - [12] R. Chen, Y.-H. Luo, J. Long, B. Shi, C. Shen, and J. Liu, Ultralow-loss integrated photonics enables bright, narrow-band, photon-pair sources, *Phys. Rev. Lett.* **133**, 083803 (2024).
 - [13] J.-Q. Wang, Y.-H. Yang, M. Li, X.-X. Hu, J. B. Surya, X.-B. Xu, C.-H. Dong, G.-C. Guo, H. X. Tang, and C.-L. Zou, Efficient frequency conversion in a degenerate χ (2) microresonator, *Phys. Rev. Lett.* **126**, 133601 (2021).
 - [14] J. Hou, J. Zhu, R. Ma, B. Xue, Y. Zhu, J. Lin, X. Jiang, Y. Zheng, X. Chen, Y. Cheng, L. Ge, and W. Wan, Enhanced frequency conversion in parity-time symmetry line, *Phys. Rev. Lett.* **132**, 256902 (2024).
 - [15] D. Renaud, D. R. Assumpcao, G. Joe, A. Shams-Ansari, D. Zhu, Y. Hu, N. Sinclair, and M. Loncar, Sub-1 volt and high-bandwidth visible to near-infrared electro-optic modulators, *Nat. Commun.* **14**, 1496 (2023).
 - [16] S. Hou, H. Hu, Z. Liu, W. Xing, J. Zhang, and Y. Hao, High-speed electro-optic modulators based on thin-film lithium niobate, *Nanomater.* **14**, 867 (2024).
 - [17] S. Xia, D. Kaltsas, D. Song, I. Komis, J. Xu, A. Szameit, H. Buljan, K. G. Makris, and Z. Chen, Nonlinear tuning of PT symmetry and non-Hermitian topological states, *Science* **372**, 72 (2021).
 - [18] H. Zhao, X. Qiao, T. Wu, B. Midya, S. Longhi, and L. Feng, Non-Hermitian topological light steering, *Science* **365**, 1163 (2019).
 - [19] N. C. Harris, G. R. Steinbrecher, M. Prabhu, Y. Lahini, J. Mower, D. Bunandar, C. Chen, F. N. Wong, T. Baehr-Jones, M. Hochberg *et al.*, Quantum transport simulations in a programmable nanophotonic processor, *Nat. Photonics* **11**, 447 (2017).
 - [20] P. A. Erdman and F. Noé, Identifying optimal cycles in quantum thermal machines with reinforcement-learning, *npj Quantum Inf.* **8**, 1 (2022).
 - [21] T. Dai, A. Ma, J. Mao, Y. Ao, X. Jia, Y. Zheng, C. Zhai, Y. Yang, Z. Li, B. Tang *et al.*, A programmable topological photonic chip, *Nat. Mater.* **23**, 928 (2024).
 - [22] Y. Yang, R. J. Chapman, B. Haylock, F. Lenzini, Y. N. Joglekar, M. Lobino, and A. Peruzzo, Programmable high-dimensional hamiltonian in a photonic waveguide array, *Nat. Commun.* **15**, 50 (2024).
 - [23] Z. Lin, W. Song, L.-W. Wang, H. Xin, J. Sun, S. Wu, C. Huang, S. Zhu, J.-H. Jiang, and T. Li, Observation of topology transition in Floquet non-Hermitian skin effects in silicon photonics, *Phys. Rev. Lett.* **133**, 073803 (2024).
 - [24] A. Gómez-León and G. Platero, Floquet-Bloch theory and topology in periodically driven lattices, *Phys. Rev. Lett.* **110**, 200403 (2013).
 - [25] A. Eckardt, Colloquium: Atomic quantum gases in periodically driven optical lattices, *Rev. Mod. Phys.* **89**, 011004 (2017).
 - [26] Q. Cheng, Y. Pan, H. Wang, C. Zhang, D. Yu, A. Gover, H. Zhang, T. Li, L. Zhou, and S. Zhu, Observation of anomalous π modes in photonic Floquet engineering, *Phys. Rev. Lett.* **122**, 173901 (2019).
 - [27] S. Yin, E. Galiffi, and A. Alù, Floquet metamaterials, *eLight* **2**, 8 (2022).
 - [28] C. Sias, H. Lignier, Y. P. Singh, A. Zenesini, D. Ciampini, O. Morsch, and E. Arimondo, Observation of photon-assisted tunneling in optical lattices, *Phys. Rev. Lett.* **100**, 040404 (2008).
 - [29] A. B. Khanikaev, S. Hossein Mousavi, W.-K. Tse, M. Kargarian, A. H. MacDonald, and G. Shvets, Photonic topological insulators, *Nat. Mater.* **12**, 233 (2013).
 - [30] Z. Yang, E. Lustig, Y. Lumer, and M. Segev, Photonic Floquet topological insulators in a fractal lattice, *Light Sci. Appl.* **9**, 128 (2020).
 - [31] W. Liu, Q. Liu, X. Ni, Y. Jia, K. Ziegler, A. Alù, and F. Chen, Floquet parity-time symmetry in integrated photonics, *Nat. Commun.* **15**, 946 (2024).
 - [32] Z. Zhang, Y. Li, X. Sun, and X. Shu, Visual observation of photonic Floquet-Bloch oscillations, *Light Sci. Appl.* **13**, 99 (2024).
 - [33] A. Dutt, M. Minkov, Q. Lin, L. Yuan, D. A. Miller, and S. Fan, Experimental band structure spectroscopy along a synthetic dimension, *Nat. Commun.* **10**, 3122 (2019).
 - [34] L. Yuan, A. Dutt, and S. Fan, Synthetic frequency dimensions in dynamically modulated ring resonators, *APL Photonics* **6**, 071102 (2021).

- [35] G. Li, Y. Zheng, A. Dutt, D. Yu, Q. Shan, S. Liu, L. Yuan, S. Fan, and X. Chen, Dynamic band structure measurement in the synthetic space, *Sci. Adv.* **7**, eabe4335 (2021).
- [36] A. Dutt, Q. Lin, L. Yuan, M. Minkov, M. Xiao, and S. Fan, A single photonic cavity with two independent physical synthetic dimensions, *Science* **367**, 59 (2020).
- [37] A. Senanian, L. G. Wright, P. F. Wade, H. K. Doyle, and P. L. McMahon, Programmable large-scale simulation of bosonic transport in optical synthetic frequency lattices, *Nat. Phys.* **19**, 1333 (2023).
- [38] I. Heckelmann, M. Bertrand, A. Dikopoltsev, M. Beck, G. Scalari, and J. Faist, Quantum walk comb in a fast gain laser, *Science* **382**, 434 (2023).
- [39] N. Englebert, N. Goldman, M. Erkintalo, N. Mostaan, S.-P. Gorza, F. Leo, and J. Fatome, Bloch oscillations of coherently driven dissipative solitons in a synthetic dimension, *Nat. Phys.* **19**, 1014 (2023).
- [40] G. Li, L. Wang, R. Ye, Y. Zheng, D.-W. Wang, X.-J. Liu, A. Dutt, L. Yuan, and X. Chen, Direct extraction of topological Zak phase with the synthetic dimension, *Light Sci. Appl.* **12**, 81 (2023).
- [41] Y. Hu, C. Reimer, A. Shams-Ansari, M. Zhang, and M. Loncar, Realization of high-dimensional frequency crystals in electro-optic microcombs, *Optica* **7**, 1189 (2020).
- [42] Y. Hu, M. Yu, N. Sinclair, D. Zhu, R. Cheng, C. Wang, and M. Lončar, Mirror-induced reflection in the frequency domain, *Nat. Commun.* **13**, 6293 (2022).
- [43] U. A. Javid, R. Lopez-Rios, J. Ling, A. Graf, J. Staffa, and Q. Lin, Chip-scale simulations in a quantum-correlated synthetic space, *Nat. Photonics* **17**, 883 (2023).
- [44] H. X. Dinh, A. Balčytis, T. Ozawa, Y. Ota, G. Ren, T. Baba, S. Iwamoto, A. Mitchell, and T. G. Nguyen, Reconfigurable synthetic dimension frequency lattices in an integrated lithium niobate ring cavity, *Commun. Phys.* **7**, 185 (2024).
- [45] Z.-A. Wang, Y.-T. Wang, X.-D. Zeng, J.-M. Ren, W. Liu, X.-H. Wei, Z.-P. Li, Y.-Z. Yang, N.-J. Guo, L.-K. Xie, J.-Y. Liu, Y.-H. Ma, J.-S. Tang, Z.-W. Zhou, C.-F. Li, and G.-C. Guo, On-chip photonic simulating band structures toward arbitrary-range coupled frequency lattices, *Phys. Rev. Lett.* **133**, 233805 (2024).
- [46] K. Wang, A. Dutt, K. Y. Yang, C. C. Wojcik, J. Vučković, and S. Fan, Generating arbitrary topological windings of a non-Hermitian band, *Science* **371**, 1240 (2021).
- [47] C. Wang, W. R. Sweeney, A. D. Stone, and L. Yang, Coherent perfect absorption at an exceptional point, *Science* **373**, 1261 (2021).
- [48] A. Li, H. Wei, M. Cotrufo, W. Chen, S. Mann, X. Ni, B. Xu, J. Chen, J. Wang, S. Fan *et al.*, Exceptional points and non-Hermitian photonics at the nanoscale, *Nat. Nanotechnol.* **18**, 706 (2023).
- [49] R. Ye, Y. He, G. Li, L. Wang, X. Wu, X. Qiao, Y. Zheng, L. Jin, D.-W. Wang, L. Yuan *et al.*, Observing non-Hermiticity induced chirality breaking in a synthetic Hall ladder, *Light Sci. Appl.* **14**, 39 (2025).
- [50] See Supplemental Material at <http://link.aps.org/supplemental/10.1103/PhysRevLett.134.163802> for construction of synthetic frequency dimension, coupled-mode theory, Floquet analysis, device fabrication, experimental setup, and time resolved transmission spectroscopy, which includes Refs. [35,51–56].
- [51] H. A. Haus, *Waves and Fields in Optoelectronics* (Prentice-Hall, Englewood Cliffs, New jersey, 1984).
- [52] B. E. A. Saleh and M. C. Teich, *Fundamentals of Photonics* (Wiley-Interscience, Hoboken, NJ, 2007).
- [53] D. Yu, B. Peng, X. Chen, X.-J. Liu, and L. Yuan, Topological holographic quench dynamics in a synthetic frequency dimension, *Light Sci. Appl.* **10**, 209 (2021).
- [54] G. Grosso and G. P. Parravicini, *Solid State Physics* (Academic Press, Singapore, 2006).
- [55] L. Yuan, Q. Lin, M. Xiao, and S. Fan, Synthetic dimension in photonics, *Optica* **5**, 1396 (2018).
- [56] L. Yuan, A. Dutt, and S. Fan, Synthetic frequency dimensions in dynamically modulated ring resonators, *APL Photonics* **6**, 071102 (2021).
- [57] V. Brasch, M. Geiselmann, T. Herr, G. Lihachev, M. H. Pfeiffer, M. L. Gorodetsky, and T. J. Kippenberg, Photonic chip-based optical frequency comb using soliton Cherenkov radiation, *Science* **351**, 357 (2016).
- [58] M. Zhang, B. Buscaino, C. Wang, A. Shams-Ansari, C. Reimer, R. Zhu, J. M. Kahn, and M. Lončar, Broadband electro-optic frequency comb generation in a lithium niobate microring resonator, *Nature (London)* **568**, 373 (2019).
- [59] S. Wan, P.-Y. Wang, M. Li, R. Ma, R. Niu, F.-W. Sun, F. Bo, G.-C. Guo, and C.-H. Dong, Self-locked broadband Raman-electro-optic microcomb, [arXiv:2405.19989](https://arxiv.org/abs/2405.19989).
- [60] L. Yuan, M. Xiao, Q. Lin, and S. Fan, Synthetic space with arbitrary dimensions in a few rings undergoing dynamic modulation, *Phys. Rev. B* **97**, 104105 (2018).
- [61] D. Cheng, E. Lustig, K. Wang, and S. Fan, Multi-dimensional band structure spectroscopy in the synthetic frequency dimension, *Light Sci. Appl.* **12**, 158 (2023).
- [62] R. Ye and G. Li, Construction of various time-varying Hamiltonians on thin-film lithium niobate chip [Dataset] (2025), [10.5281/zenodo.15086325](https://zenodo.org/record/15086325).